Two Dimensional Galaxy Image Decomposition

Yogesh Wadadekar,[1] Braxton Robbason [2] and Ajit Kembhavi [3]
Inter University Centre for Astronomy and Astrophysics, Post Bag 4, Ganeshkhind, Pune 411007, India

ABSTRACT

We propose a two dimensional galaxy fitting algorithm to extract parameters of the bulge, disk, and a central point source from broad band images of galaxies. We use a set of realistic galaxy parameters to construct a large number of model galaxy images which we then use as input to our galaxy decomposition program to test it. We elucidate our procedure by extracting parameters for 3 disk galaxies – NGC 5326, NGC 5587 and NGC 7311 and compare our results with those previously reported in the literature.

Subject headings: galaxies: fundamental parameters — galaxies: spiral — galaxies: structure

1. Introduction

The luminosity profile of a typical spiral or S0 galaxy most often contains two components, a spheroidal bulge and a circular disk. If the galaxy possesses an active nucleus, then a high central point intensity may also be present. The projected bulge intensity profile is usually represented by an $r^{1/4}$ law (de Vaucouleurs 1948), where r is the distance along the major axis. In recent times, a generalised $r^{1/n}$ law is increasingly being used. The intensity profile of the disk component is usually represented by an exponential (Freeman 1970). These profiles are entirely empirical, and have not been derived from a formal physical theory. However, numerical simulations in simplified situations such as those by Van Albada (1982) have been able to recreate $r^{1/4}$ profiles for the bulge.

The photometric decomposition of galaxies into bulge and disk and the extraction of the parameters characterizing these components has been approached in a number of ways. Early attempts at such decomposition assumed that the disk would be the dominant component in the outer regions of galaxies and that the bulge would dominate the inner regions. Disk and bulge parameters were extracted by Kormendy (1977) and Burstein (1979) by fitting for each component separately in the region in which it was dominant. Kent (1985) first introduced simultaneous fitting of bulge and disk components to major and minor axis light profiles of galaxies obtained by fitting ellipses to the isophotes of CCD images. One major advantage of Kent's method is its ability to extract galaxy parameters in a model independent way provided that the disk and the bulge have very different ellipticities. His method works well for edge on galaxies where the ellipticity of the disk is generally much higher than the ellipticity of the bulge. Schombert and Bothun (1987) employed a similar technique for initial estimation of bulge and disk parameters of simulated galaxy profiles, with standard laws describing the bulge and the disk with simulated noise. These parameters were then used as initial input to a χ^2 fitting procedure. Tests on simulated profiles indicated good recovery

[1]yogesh@iucaa.ernet.in

[2]Current Address: Harvard University, robbason@head-cfa.harvard.edu

[3]akk@iucaa.ernet.in

of both bulge and disk parameters [4]. These techniques of fitting standard laws to a 1-D intensity profiles extracted from galaxy images were critically examined by Knapen and van der Kruit (1991). They found that even for the same galaxy different authors derive disk scale length values with an average scatter as high as 23%. Such large uncertainty in the extracted structural parameters is a hindrance in the study of structure, formation and evolution of the bulge and disk of galaxies. Accurate, reliable determination of parameters is a prerequisite for differentiating between competing galaxy formation and evolution models. The conventional one dimensional technique is also limited because it assumes 1-D image profiles can be uniquely extracted from galaxy images. This is not possible if a strong but highly inclined disk is present.

Andredakis, Peletier and Balcells (1995, henceforth APB95) used a 2-D generalisation of Kent's method to fit K-band luminosity profiles of bulges of a sample of disk galaxies with morphological types ranging from S0 to Sbc. They used azimuthally averaged profiles from various radial cuts of the image of the galaxy. An important innovation in this paper was the use of a $r^{1/n}$ law for the bulge. A full two dimensional technique which uses the entire galaxy image rather than one dimensional profiles was proposed by Byun and Freeman (1995, henceforth BF95). A similar approach was used by R. S. de Jong to extract parameters for a sample of 86 face on disc dominated galaxies (de Jong 1996, henceforth DJ96). In this paper, we describe a 2-D decomposition technique similar to the one employed in BF95. Extending that work, we fit for a central point source in addition to a bulge and disk. In addition, our method takes into account the effects of convolution with the PSF and photon shot noise from the sky background and the galaxy. We also use the $r^{1/n}$ law for the bulge as in APB95. We try to quantify effects of other features such as foreground stars on parameter extraction. We illustrate the efficacy of our methods by extracting bulge and disk parameters for three galaxies chosen from the data in APB 95. We also briefly discuss reliability of error bar estimates on parameters extracted.

In Section 2, we describe our method of constructing artificial galaxy images as test cases for our bulge–disk decomposition procedure and in Section 3 the decomposition procedure. Section 4 is a detailed analysis of the testing we performed to test our decomposition algorithm, using simulated galaxy images. Section 5 is a description of application of the technique to three galaxies and a comparison of the results with previously published values. Section 6 contains a discussion about error bars on the parameters extracted and Section 7 contains the conclusions.

2. Simulation of Galaxy Images

In order to test the decomposition procedure, we have developed a simulation code to generate galaxy images closely resembling those obtained using CCD detectors on optical telescopes. Using the code it is possible to simulate a CCD image of a galaxy with desired bulge, disk and point components at any position and orientation on the CCD. The image can be convolved with a circular gaussian PSF and Poisson noise can be added if required. Stars can be introduced into the image at random positions and additional features such as absorbing dust lanes can be added. All parameters used by the program to generate these features can be easily modified by the user through a parameter file.

Galaxy profiles are the projections of three dimensional luminosity profiles onto the plane of the sky. The disk is inherently circular, so it projects as an ellipse. The inclination angle of the disk with respect to the plane of the sky completely determines its ellipticity in the image. Bulges, taken to be triaxial ellipsoids

[4]For a review of various 1-D decomposition techniques see Simien (1989).

in the general case, also project as ellipses but the ellipticity of the bulge does not reach such high values as the disk. For a triaxial ellipsoid with major axis a, minor axis b, and an intermediate axis c, the highest possible ellipticity is $1 - b/c$. Therefore the projected galaxy shows elliptical bulge isophotes and, in many cases, more elliptical disk isophotes.

At a given point on the image plane, contribution to the intensity from the bulge and the disk depends on their respective central intensities, ellipticities and scale lengths. Near the galaxy center there is an additional contribution from the point source, if one is present.

In our galaxy simulation, the projected bulge component is represented by the $r^{1/n}$ law with effective (half light) radius r_e (which is the radius within which half the total light of the galaxy is contained), intensity at the center of the galaxy I_0 and a constant ellipticity $e_b = 1 -$ (minor axis length/major axis length):

$$\begin{aligned} I_{bulge}(x,y) &= I_0 e^{-2.303b(r_{bulge}/r_e)^{1/n}}, \\ r_{bulge} &= \sqrt{x^2 + y^2/(1-e_b)^2}, \end{aligned} \tag{1}$$

where x and y are the distances from the center along the major and minor axis respectively and b is the root of an equation involving the incomplete gamma function $P(a,x)$:

$$P(2\,n, 2.303\,b) = 0.5,$$

This equation can be solved numerically as we do in our code. However, a simplification can be introduced in the procedure because the b and n values satisfy the relation:

$$b = 0.8689n - 0.1447$$

The projected disk is represented by an exponential distribution with central intensity I_s, scale length r_s and a constant ellipticity e_d,

$$\begin{aligned} I_{disk}(x,y) &= I_s e^{-r_{disk}/r_s}, \\ r_{disk} &= \sqrt{x^2 + y^2/(1-e_d)^2}. \end{aligned} \tag{2}$$

The disk is inherently circular. The ellipticity of the disk in the image is due to projection effects alone and is given by:

$$e_d = 1 - \cos(i) \tag{3}$$

where i is the angle of inclination between the line of sight and the normal to the disk plane. Finally, the point source is represented by an intensity added to the central pixel of the galaxy prior to convolution with the PSF. Foreground stars are added at random positions as intensities at a single pixel prior to convolution with the PSF. The convolution with the PSF is performed in the Fourier domain. For adding photon shot noise, a constant sky background is added to every pixel. The resultant count (which includes intensity from the galaxy as well as the sky background) is multiplied by the gain (electrons/ADU). A random Poisson deviate about this value is obtained. The deviate is then divided by the gain and the background is subtracted out.

The program takes about 3 seconds to generate a 256 × 256 pixel galaxy image, when running on a SUN UltraSparc 1. A copy of this code (written entirely in ANSI C) is available upon request.

3. 2-D Decomposition Technique

3.1. Building The Model

The 2-D decomposition technique involves building 2-D image models that best fit the observed galaxy images. The model to be fit is constructed using the same procedure as the simulated images described in the previous section, except that features of the image that are not contributed by the galaxy such as Poisson noise are not added. The galaxy position and position angle are *not* parameters that are fitted for in our decomposition. The position angles of the bulge and the disk are also assumed to be identical.

3.2. The Decomposition Procedure

To effect the decomposition, we attempt to iteratively minimize the difference between our model and the observed galaxy (or a simulated one), as measured by a reduced χ^2_ν value. For each pixel the observed galaxy counts are compared with those predicted by the test model. Each pixel is weighted with the variance of its associated intensity as determined by photon shot noise of the combined sky and galaxy counts at that pixel. This weightage scheme has been used as it gives importance to pixels in proportion to their signal to noise ratio. Our scheme makes the fit less sensitive to the contribution of the bulge in the outer region of the galaxy where the disk dominates. Thus an effect similar to the earlier decompositions where the disk was fitted to the outer region and a bulge to the inner region of the galaxy is obtained automatically. Since photon shot noise obeys Poisson statistics the variance is equal to the intensity value. Hence

$$\chi^2_\nu = \frac{1}{\nu} \sum_{i,j} \frac{[I_{model}(i,j) - I_{obs}(i,j)]^2}{I_{obs}(i,j)}, \tag{4}$$

where i, j range over the whole image, $\nu = N-$ (number of fitted parameters) is the number of degrees of freedom with N being the number of pixels in the image involved in the fit, and I_{obs} is assumed to be greater than zero in all cases.

For real galaxies, our decomposition program assumes that pixel values I represent real photon counts. If the image has been renormalized in any way (divided by the exposure time for example), the extracted χ^2_ν value should be multiplied by the appropriate factor to account for that normalization.

Eight fitting parameters are used in our scheme. These are $I_0, I_s, r_e, r_s, n\ e_b, e_d$, and a central point source intensity I_p. The first 4 parameters were used by Schombert and Bothun (1987), and parameters 1 to 4 along with parameters 6 and 7 were used by the authors of BF95 and DJ96. We have added capability in our code to fit for position angle and a constant background, although the background is not fitted for in the simulations reported here. During our preprocessing we estimate the background carefully and subtract it out. CCD images of galaxies contain features such as foreground stars and bad pixels that may contaminate the decomposition procedure. In the case of real galaxies, we take care to mask out bad pixels and visible foreground stars before commencing decomposition.

The minimization uses MINUIT 94.1, a multidimensional minimization package from CERN, written in standard FORTRAN 77. MINUIT allows the user to set the initial value, the resolution, and the upper and lower limits of any parameter in the function to be minimized. Values of one or more parameters can be kept fixed during a run. MINUIT can use several strategies to perform the minimization. Our choice is

MIGRAD, a stable variation of the Davidon–Fletcher–Powell variable metric algorithm. It calls the user function (in our case χ^2_ν) iteratively, adjusting the parameters until certain criteria for a minimum are met. Our code typically takes 0.03 seconds per iteration on a Ultra Sparc 1 workstation, when working on a 64 $\times$ 64 pixel galaxy image. Since we are using fast Fourier transforms to convolve the model with a gaussian PSF, the execution time can be expected to scale as $N \log N$, with N the total number of pixels in the image. We do find that execution time scales almost linearly with the number of pixels in the image. About 2000 iterations are required for convergence criteria to be satisfied when all 8 parameters are kept free, so a typical run takes about one minute. Computation time is reduced as the number of free parameters are reduced.

A copy of this code (written mostly in ANSI C with some optional display routines in IDL) is available upon request.

4. Reliability of Galaxy Image Decomposition

We have conducted elaborate tests of the effectiveness of the program in extracting parameters under different input conditions.

4.1. Large-Scale Testing under Idealized Conditions

We expect that our method can be used for unsupervised, automatic parameter extraction for large sets of galaxies. To test the accuracy and reliability of our decomposition procedure, we constructed image sets of 500 model galaxies with an absolute magnitude of -21 with random uniform selection of disk to bulge ratio, scale lengths, bulge parameter n and ellipticities. The ranges we used for each parameter are,

$$\begin{aligned} 3 < \quad & r_e \quad < 10 \text{ kpc}, \\ 0.0 < \quad & e_b \quad < 0.4, \end{aligned}$$

for the bulge and

$$\begin{aligned} 0 < \quad & D/B \quad < 3, \\ 3 < \quad & r_s \quad < 15 \text{ kpc}, \\ 0 < \quad & e_d \quad < 0.8. \end{aligned}$$

for the disk.

The ranges chosen for the parameters encompass most values encountered in real galaxies with Hubble types ranging from E to Sb. All simulated galaxies were assumed to be at a redshift of 0.15. The pixel scale used was 0.5 arcsecond/pixel, CCD gain was 1.0 ADU/electron, FWHM of the PSF was 1.0 arcseconds and the value of the Hubble constant used was $H_0 = 100\,\mathrm{km\ sec^{-1}\ Mpc^{-1}}$. We used a sky background value of 21.9 magnitudes/(arcsecond)^2. This corresponds to the value of the sky background measured in the V filter at KPNO (Massey Gronwall and Pilachowski, 1990). The sky background was estimated in a trial run

and then held fixed to that value thereafter. It was not a free parameter in these simulations. The scaling used to convert apparent magnitudes to CCD counts was estimated using photometric data on a 1m class telescope. On such a telescope, an exposure time of about 30 minutes would be required to get the S/N ratio used in these simulations. The galaxies generated by the galaxy simulation program were then used as input to the bulge disk decomposition program. We studied how accurate and reliable the decomposition program is in recovering the input parameters.

In the first set of trials, we generated 500 galaxies with $n = 4$. During the extraction, the parameter n was held fixed at a value of 4. We placed no additional relative constraints on permissible parameter values such as those used in BF95. We found that the χ^2_ν for the fits is worse than 2 in 120 cases out of 500, giving a 24% failure rate. These failures are all caused by one or more parameters hitting their limits, causing the gradient-driven minimization routine to fail. It is possible for us to reduce the failure rate to about 10% by carefully changing starting values and parameter ranges by trial and error. In every case of failure due to parameters hitting limits, MINUIT generates appropriate warning messages, so there is no danger that such failures will contaminate the good results. The failure rate decreases as the number of free parameters decreases. It is possible to completely eliminate such failure by changing the initial value and constraining the range of parameters narrowly around the *expected* value which we have knowledge of, in the case of a simulation. While dealing with real galaxies, in case of a failure to obtain a satisfactory fit, the situation could be addressed by trying different initial values and ranges, with guesses based on inspection of the intensity profile. We find that a $\chi^2_\nu < 2$ almost always corresponds to good recovery of input parameters, and a $\chi^2_\nu > 2$ always corresponds to poor recovery of input parameters. Poor recovery of one parameter almost always implies poor recovery of all other parameters, a high value of χ^2_ν and at least one parameter hitting limits. In such a case, one would need to use a new set of starting values and parameter ranges and try again. It should be noted that failure in recovering parameters is easy to detect as it is always flagged by a high χ^2 value.

The extracted versus input data have been plotted in Fig. 1, with points having $0 < \chi^2_\nu < 2$ marked with a $\circ$, while the remaining points are marked with a dot. Note that the points with a bad fit (i.e. $\chi^2_\nu > 2$) generally lie far away from the line on which the input value equals the extracted value. Almost all the remaining points (those with $0 < \chi^2_\nu < 2$) plotted on these graphs are tightly grouped along this line. The authors of APB 95 report that the ellipticity of the bulge is not easy to determine by any method, and errors of the order of 30% are possible. Our method however, seems to recover bulge ellipticity to a high degree of accuracy.

In a second set of 500 runs, we varied n in the range

$$1.0 < \quad n \quad < 6.0$$

All other parameters were varied within the same ranges specified above. In this case, the failure rate was 25%. The extracted versus input data have been plotted in Fig. 2. As before, points with $\chi^2_\nu > 2$ are marked with a dot. Points with $\chi^2_\nu < 2$ and $n < 4$ are marked with a $\circ$ while points with $\chi^2_\nu < 2$ and $n > 4$ are marked with a Δ. There is a marked increase in scatter of all parameters as compared to the $n = 4$ case described above, even for points with $\chi^2_\nu < 2$. Most significantly, the scatter in the extraction of n is rather large for $n > 4$. This occurs because the intensity profile of the bulge gets steeper as n increases. For large n the fall-off in intensity with distance from the center is so rapid, that hardly any points with good S/N are available, for fitting the bulge of the galaxy. This leads to larger errors in estimation of n and other bulge parameters, contributing to the increased scatter seen in n, disk to bulge ratio and bulge scale length for

$n > 4$. The only way to reliably extract the bulge profile for galaxies with a weak bulge resulting from an unfortunate combination of small bulge scale length, high D/B and large n is to use a higher exposure time to improve S/N. When we increased the exposure time by a factor of ten, there was a noticeable decrease in scatter for large n. In most real situations where it is not feasible to increase exposure time, it should be borne in mind that extracted values with large n and/or small bulge scale lengths are prone to error.

4.2. Tests of stability

We conducted a series of tests to determine how the program responds to deviations from the idealized conditions assumed in the previous section, to gain some insight into problems encountered when dealing with real galaxy images rather than simulated ones.

4.2.1. Effect of changing S/N ratio

The S/N ratio improves with increase in exposure time. We examined the image of the same simulated galaxy using pixel counts for a bright galaxy and sky background corresponding to exposure times ranging from about 5 seconds to 8 minutes on a 1 m class telescope. The exposure times (and hence the pixel counts) varied by a factor of 96 and S/N ratio by a factor of about 10 ($\simeq \sqrt{96}$). The background counts used were estimated from observations made on a 1m class telescope in the Cousins R filter. We expected that as S/N got better, the fit would improve and parameter recovery would get more accurate. We found that the accuracy of the extracted parameter values is strongly dependent on the exposure time only for short exposures of < 30 seconds. The results for different exposure times are shown in Table 1 which compares various input values of intensity at the effective radius I_e with the corresponding extracted value. Peak counts of less than one thousand for galaxies are not very useful for the purpose of bulge disk decomposition.

It is seen that χ^2_ν *increases* slowly but monotonically with exposure time. This is an artifact of the way sky background is used in the program creating the input galaxies. When simulating galaxies, background is added, Poisson noise is calculated using the intensity of both background and galaxy, and the background is subtracted out. Then, when the fitting program runs, it estimates the noise at each pixel as the square root of the number of counts at that pixel, but the actual noise is the square root of the sum of the number of counts and the background. This causes the points with low counts to be weighted more than they should be (resulting in higher χ^2_ν), but the difference is small.

4.2.2. Effect of erroneous measurement of PSF

With real data it is often impossible, even if a large number of stars are used, to measure the FWHM of the PSF to an accuracy of better than about 5%. One reason for this is the variation of the PSF over different regions of the CCD. Therefore, it is important to know how the fit will react to an over– or under–estimation of the FWHM of the PSF, and to an elliptical PSF. The value of the point source is expected to be affected the most because of errors in PSF estimation. If the bulge scale length r_e is very small, then bulge parameters will also be seriously affected by an incorrect estimation of the PSF. We ran two separate tests, one with a circular PSF, with the FWHM overestimated or underestimated by up to

20%, and another where the width along one axis of the PSF changed by 20% while the other remained constant, thereby generating elliptical PSFs. During the fitting we used a constant circular Gaussian PSF with FWHM $\Gamma_{fit} = 1$ pixel in all the test cases described below.

For these tests, our simulated images were generated using a PSF with varying FWHM, denoted by Γ_{image}. $\Gamma_{image}/\Gamma_{fit} \neq 1$ corresponds to the situation where an error is made in the estimation of the FWHM of the PSF used in modeling the intensity distribution of observed galaxies. In the first test we assumed that the PSF shape is circular and the only error is in estimating the value of the FWHM. When $\Gamma_{image}/\Gamma_{fit} < 1$ the spreading of the image due to seeing is overestimated by the decomposition program. The excess deconvolved intensity at the center causes it to report a fictitious point source. The minimum value for the ratio we have used in the test is 0.8. At this ratio, the fitted intensity of the fictitious point source is very high, as can be seen from Fig. 3. The bulge intensity is at its minimum value. The intensity of the fictitious point source decreases and that of the bulge increases continuously as $\Gamma_{image}/\Gamma_{fit} \rightarrow 1$. If the FWHM of the PSF is underestimated, i.e. $\Gamma_{image}/\Gamma_{fit} > 1$, the point intensity becomes negative[5]

The variation $\Gamma_{image}/\Gamma_{fit}$ did not affect the extracted disk scale length, which only once deviated by more than 1 pixel. The disk intensity increased with increasing input PSF, analogous to the increase in bulge intensity discussed above. The extracted bulge and point source intensities, and bulge radius, all vary systematically and approximately linearly with the error in PSF estimation. χ^2_ν is very good in all cases, decreasing somewhat as the PSF gets to be closer to our estimate of 1. These results are plotted on the left panel of Fig. 3.

To see the effect of errors in determining the shape of the PSF, we generated galaxies with different elliptical PSFs. Such PSFs are observed, for example, if the plane of the CCD is inclined to the focal plane of the telescope. The decomposition program continued to use a fixed circular PSF. The sequence of image PSFs was generated by keeping one of the principal axes of the ellipses always equal to Γ_{fit}, and varying the other principal axis so that ratio of the two changed from 0.8 to 1.2. The results of parameter extraction are plotted on the right panel of Fig. 3, as a function of $\Gamma_{image}/\Gamma_{fit}$, where the ratio is now taken along the changing principal axis.

When the PSFs used in the simulation as well as fitting are both circular, but have different Γ_{image}, the fitting procedure leads to a positive or negative fictitious point source. A good overall fit is obtained with χ^2_ν close to unity in the latter case, i.e. when $\Gamma_{image}/\Gamma_{fit} > 1$, because here the overall intensity at the centre remains small and best fit bulge parameters which give a good fit, together with the negative point source can be found. In the case of a positive point source, changed bulge parameters cannot compensate for the error in the PSF and the quality of the fit is diminished. In the case of the elliptical PSFs, χ^2_ν is greater than unity on both sides of $\Gamma_{image}/\Gamma_{fit} = 1$.

Bulge ellipticity, which was set to 0.1 in all simulated images, was extracted very well in the case of the circular PSF as it varied over its range of FWHM. When the PSF becomes elliptical, we expect the extracted ellipticity to increase as well, and it does, but only to 0.12 for the most elliptic PSF, which had ellipticity 0.2. The ellipticity close to the centre of the galaxy is of course wholly determined by the shape of the PSF, while further away, the effects on the extracted ellipticity are much smaller.

---

[5]A negative point is non physical, of course, but in general we will allow for it because the law describing the bulge does not hold near the center of most galaxies. In our simulation however we have assumed that the law holds right to the center.

4.2.3. Fitting in the presence of stars

Our aim here was to check if the presence of bright foreground stars on the galaxy could cause a systematic deviation in extracted parameters. To test this, we added upto 20 randomly positioned stars to a 128 × 128 pixel image, and ran the decomposition program without blocking out the stars. The presence of the stars worsened the χ^2 considerably but the extracted parameters were not affected in any significant or systematic way. Masking out the stars improved the χ^2 to normal values (≈ 1), and the parameters were also accurately extracted as before.

4.3. Detecting a point source

We have examined the extraction of a point source at the centre of the galaxy. Since the bulge intensity has a very sharp peak near the center, a point source can be easily swamped by the bulge unless it is very bright. The objective here is to find powerful sources, and not very weak ones where the point intensity is less than the bulge intensity at the central pixel. We looked at various strengths of the point relative to the bulge, by examining a uniform grid of 5 × 5 values of point and bulge central intensities, over which the bulge and point each varied by a factor of thirty. There was no detection of a fictitious point. Weak points were absorbed into the bulge, while strong points were extracted well, as shown in Fig. 4. For higher bulge intensities, the point intensity was extracted better, because higher S/N far from the center served to constrain the bulge intensity more precisely.

5. Fitting real galaxy images

The ultimate goal of this program is to extract parameters from a large sample of galaxies of different morphological types of the kind reported in APB95, RF96 and Byun (1992). To elucidate what our program can do, and to compare results with those obtained by other workers, we have used our program to extract parameters for three disk galaxies chosen from the data in APB95. Our program does not model bars, spiral arms and such other features, so we chose galaxies where these features did not dominate when the images were visually inspected. We used the online data available at http://www.elsevier.nl/locate/newast and described in Peletier and Balcells (1997). More extensive work on the larger samples will be reported separately. Here we wish to merely compare the results of our approach with that reported in APB95.

5.1. Possible pitfalls

Going from fitting simulated models to fitting real galaxies has several attendant dangers. Significant errors in the PSF can cause the detection of a fictitious point source (Section 4.2.2). Since the PSF is never known exactly, any extraction of a point must be examined very carefully. HST data shows that a single power law describing the bulge is a poor approximation to to the intensity profile near the center of the galaxy (Byun et al 1996). Without very precise knowledge of the PSF, measuring systematic deviations from the law is not reasonable. Images are often normalized, averaged, or background subtracted during processing. Knowledge of the normalization used is required before we get an accurate estimate of the S/N ratio which is a prerequisite for determining the weighting function for our χ^2 minimization.

In extreme cases, the luminosity distribution of two physically different components are very similar

and they can give very similar values of reduced χ^2. Our method can give incorrect results under such circumstances. For example, a bulge with a very small scale length can be easily confused with a point source. Similarly a extremely large but weak circular disk can appear like background sky. High redshift galaxies with small scale length in angular terms do not have sufficient number of high S/N pixels for a reliable fit.

5.2. Comparison of extracted parameters

Table 2 shows extracted values from our program, as compared with values published in APB95 for three disk galaxies NGC 5326, NGC 5587 and NGC 7311. Both the bulge and disk ellipticities match very well. Correct extraction of ellipticities is a prerequisite for the APB95 method of decomposition to work but is not required in our method. In two out of three cases, the discrepancy in n is larger than the error bar reported in APB95 but the deviation is not large. There is discrepancy in the value of bulge scale length of a factor of almost exactly ~ 2.5. We are unable to account for this discrepancy. We have also reported the disk scale length for these galaxies, which is held fixed at 25 arcsecond for all galaxies in APB95. In Table 2 we have converted the angular scale length reported in APB95 to a linear scale. Our extracted values for disk scale length match those in APB95 to within a factor of two.

It should be noted that our technique is fundamentally different from that used in APB95. We use the 2-D images directly, not azimuthally averaged luminosity profiles. Our method extracts all galaxy parameters at one go, with no prior knowledge of ellipticities. We expect our method to work well for disk galaxies at any orientation.

6. Error estimation

In minimization problems, two methods are commonly employed for parameter error estimation. The first is to estimate the error from the second derivative of the function being minimized with respect to the parameter under consideration. The second is to gradually move away from the the minimum until a predetermined χ^2 is exceeded. The second method will work for a single parameter fit irrespective of whether the χ^2 function near the minimum is parabolic in shape, or of a more complicated nature. MINUIT can perform error estimations using both methods.

In any multi–parameter minimization process, formal errors on the parameters can be generated from the the covariance matrix of the fit only if: (i) the measurement errors are normally distributed and either, (ii-a) the model is linear in its parameters or (ii-b) the sample size is large enough that the uncertainties in the fitted parameters do not extend outside a region where the model could be replaced by a suitable linearized model. It should be noted that this criterion does not preclude the use of a non-linear fitting technique to find the fitted parameters (Press et al, 1992).

Amongst the bulge and disk parameters that we use in the fit, two are linear (I_0 and I_s) and the rest are non-linear. Non-linearity is highest for e_b and e_d. Leaving all parameters free results in rather large formal error bars on extracted parameters (20- 30%). The χ^2 function is not parabolic near the minimum, which causes incorrect error estimation by MINUIT when the derivative method is used. Even moving away from the minimun until some χ^2 is exceeded does not work here as there are multiple free parameters that are correlated. MINUIT is therefore unable to compute errors using this technique when all parameters are

free. Fixing the most non-linear parameters i.e. the ellipticities to their extracted value enables MINUIT to compute formal errors using this technique as the function can be approximated by a linearized model. The errors are however still large. Fixing more parameters reduces the error bars. Formal errors match those obtained from parameter recovery in the 500 model test if only *one* parameter is left free. Given the strong inherent non-linearity of our model, the problem of obtaining formal error bars on extracted parameters, when more than one parameter is left free simultaneously, will be mathematically difficult.

7. Conclusions

Unprecedented amounts of CCD imaging data on galaxies will be generated by ongoing surveys such as the Sloane Digital Sky Survey. Analysis of these data will require completely automated, fast and reliable algorithms for tasks such as morphological classification (eg. Abraham et al. 1994) followed by bulge–disk decomposition for an appropriate subset of galaxies. Extensive tests on simulated galaxy images show that the two dimensional fitting procedure described here is very successful at accurately extracting a wide range of input parameters, and that the cases where it fails can be easily detected from the χ^2 value since failure is always accompanied by a high χ^2 value.

One major limitation of our method is that it assumes that the observed luminosity profile of the galaxy under consideration actually follows the empirical laws we have chosen irrespective of the great variation seen in galaxy morphologies. Studies of the effects of morphological features such as dust absorption in disks modeled by Evans (1982) on scale parameters are required if we are to develop a reliable methodology to extract parameters for galaxies with strong features such as bars, spiral arms etc.

For galaxies with very steep luminosity profiles (i.e. small bulge scale length or large n), conventional 1-D fitting may provide a better solution than 2-D methods because in such galaxies, a very large fraction of pixels have poor signal to noise. This works against a good determination by the 2-D method, which uses individual pixels over the whole image in the fit. When there is large isophotal twist in the galaxy, a 1-D method may work better than the 2-D one, because most 1-D methods follow the twisting of the ellipses by changing the position angle with radius. All 2-D methods proposed to date hold the position angle constant. When effects of shape parameters are significant, a 2-D technique is better. For example when a highly inclined disk is present, 1-D fits might miss it altogether, or provide a very poor fit. 2-D methods are also better in extraction of ellipticities of the bulge and the disk, and for extraction of the point source, as the larger number of data points available help constrain the extracted value better.

Our extracted galaxy parameters are consistent with those reported in APB95. Our method does not require galaxies to have significantly different bulge and disk ellipticities as required in the mehod described in APB95. Thus it is well suited for decomposition of face–on as well as edge–on disk galaxies. We wish to sound a note of caution about the lack of reliability of bulge disk decomposition for galaxies with strong features such as a bar or spiral arms, those with $n > 4$ and those with a poorly estimated PSF. Although a good fit can be probably be obtained even for such galaxies using our method, our χ^2 value would no longer be a powerful tool to distinguish between good and bad fits. We intend to apply our technique to a sample of low redshift elliptical galaxies currently being studied by us.

We thank Ashish Mahabal, S. K. Pandey and Tushar Prabhu for helpful comments and discussions. We thank Y. C. Andredakis, R.F. Peletier and M. Balcells for making their data publicly available. We thank an anonymous referee whose insightful comments helped improve this paper.

REFERENCES

Abraham, R.G., Valdes, F., Yee, H.K.C., & van den Bergh, S. 1994, ApJ, 432, 75
Andredakis, Y.C., Peletier, R.F., & Balcells, M. 1995, MNRAS, 275, 874
Burstein, D. 1979, ApJ, 234, 435
Byun, Y.I., & Freeman, K. 1995, ApJ, 448, 563
Byun, Y.I. *et al* 1996, AJ, 111, 1889
de Jong R. S. 1996, A&AS, 118, 557
de Vaucouleurs, G. 1948, Ann. d'Astrophys., 11, 247
de Vaucouleurs, G. *et al*, 1991, Third Reference Catalog of Bright Galaxies (New York: Springer)
Evans, R. 1994, MNRAS, 266, 511
Freeman, K. 1970, ApJ, 160, 811
Kent, S.M. 1985, ApJS, 59, 115
Kormendy, J. 1977, ApJ, 217, 406
Knapen, J. H., & van der Kruit, P. C. 1991, A&A, 248, 57
Massey, P., Gronwall, C., & Pilachowski, C. A. 1990, PASP, 102, 1046
Peletier, R.F., & Balcells, M. 1997, New Astronomy, 1, 349
Press, W.H., Teukolsky, S. A., Vetterling, W.T., & Flannery, B.P. 1992, Numerical Recipes in C (Cambridge: Cambridge University Press)
Schombert, J., & Bothun, G. D. 1987, AJ, 93, 60
Simien, F. 1989, in Le Monde des Galaxies, ed. H.G. Corwin, Jr. & L. Bottinelli (Berlin:Springer), 293
Van Albada, T. S. 1982, MNRAS, 201, 939

Table 1: Effect of changing exposure time

Exp. time (sec)	χ^2_ν	Peak Counts	Input I_e	Extracted I_e	% Error in I_e
5	1.00	302	4.17	6.4	53.0
15	1.00	914	12.50	11.1	8.9
30	1.02	1923	25.00	24.2	3.2
60	1.04	3665	50.00	51.2	2.4
120	1.07	7623	100.00	101.0	1.0
240	1.11	14826	200.00	202.0	1.0
480	1.14	29740	400.00	415.0	3.8

Table 2: Comparison of extracted parameters

Parameter	Source	NGC 5326	NGC 5587	NGC 7311
Bulge ellipticity	APB95	0.20	0.20	0.00
	This paper	0.31±0.13	0.22± 0.18	0.07 ± 0.34
Disk ellipticity	APB95	0.55	0.70	0.53
	This paper	0.55± 0.05	0.78± 0.20	0.56 ± 0.06
D/B	APB95	4.00	20.00	5.26
	This paper	3.04	26.48	4.38
n	APB95	2.19 ± 0.45	1.53 ± 0.21	1.32 ± 0.12
	This paper	1.78± 0.12	2.10 ± 0.16	1.90± 0.13
Bulge Scale length (kpc)	APB95	0.54	0.48	0.87
	This paper	0.22± 0.03	0.20± 0.03	0.34± 0.04
Disk Scale Length (kpc)	APB95[a]	1.69	1.93	3.60
	This paper	0.74± 0.05	1.64± 0.19	1.62± 0.16

[a]Disk scale length was held fixed at 25 arcsecond for all galaxies in APB95

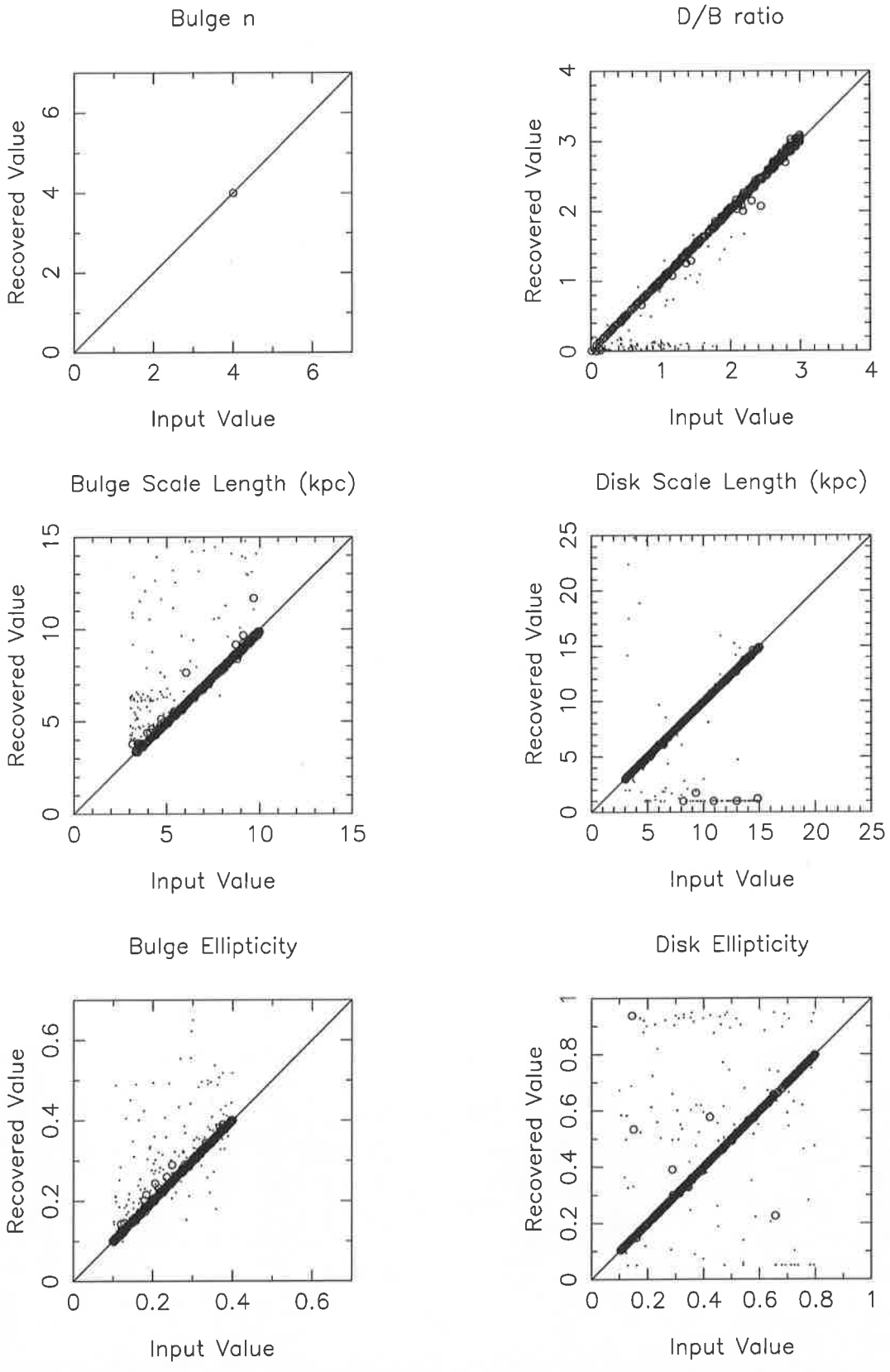

Fig. 1.— Scatter plots of extracted versus input parameters for galaxies with $n = 4$. Points with $0 < \chi^2_\nu < 2$ are indicated by a ∘ while those with $\chi^2_\nu > 2$ are indicated by a dot.

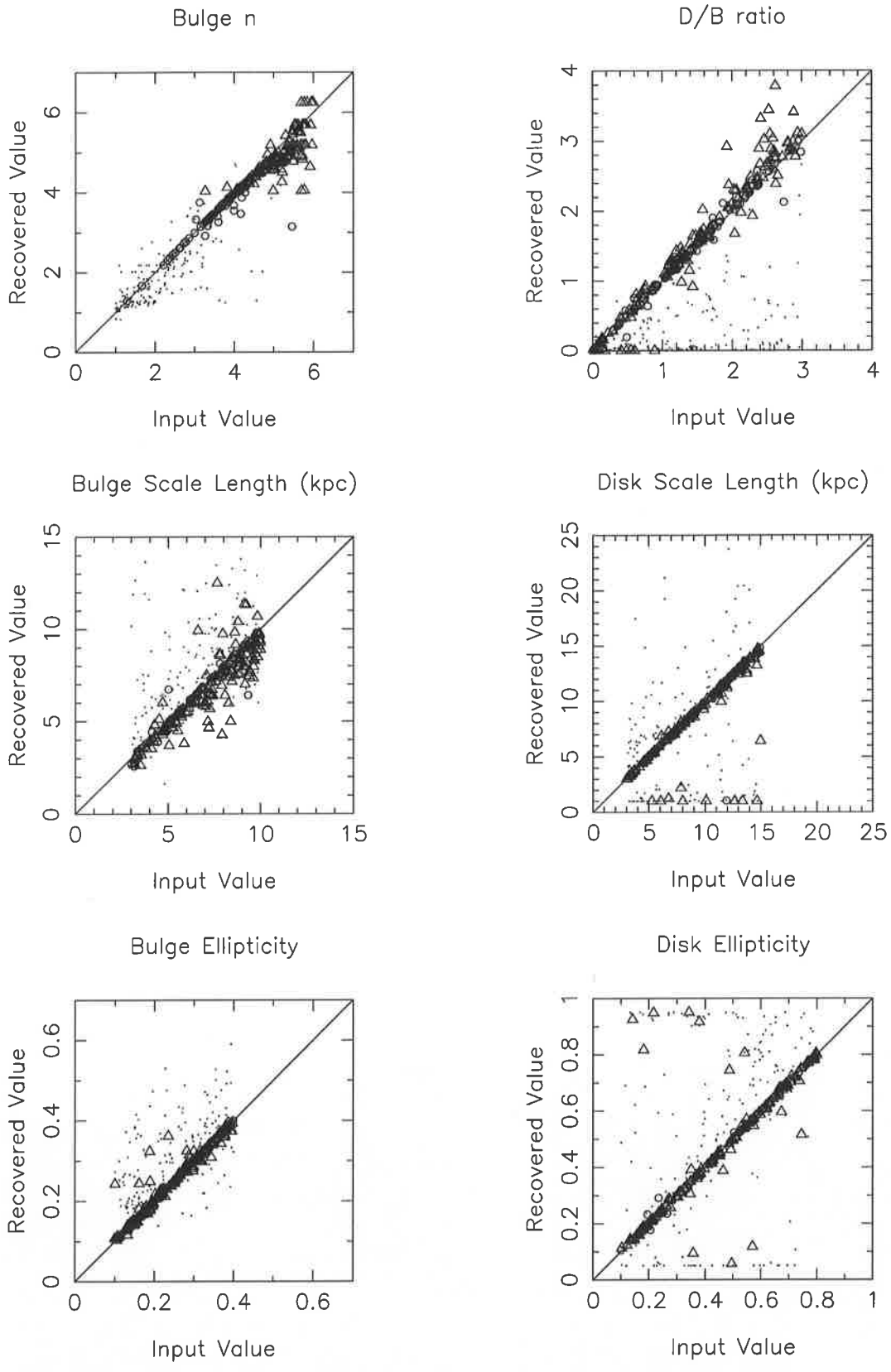

Fig. 2.— Scatter plots of extracted versus input parameters with n in the range $1.0 < n < 6.0$. Points with $\chi^2_\nu > 2$ are indicated by a dot while those with $0 < \chi^2_\nu < 2$ are indicated by a $\circ$ or a $\triangle$. See the text for details.

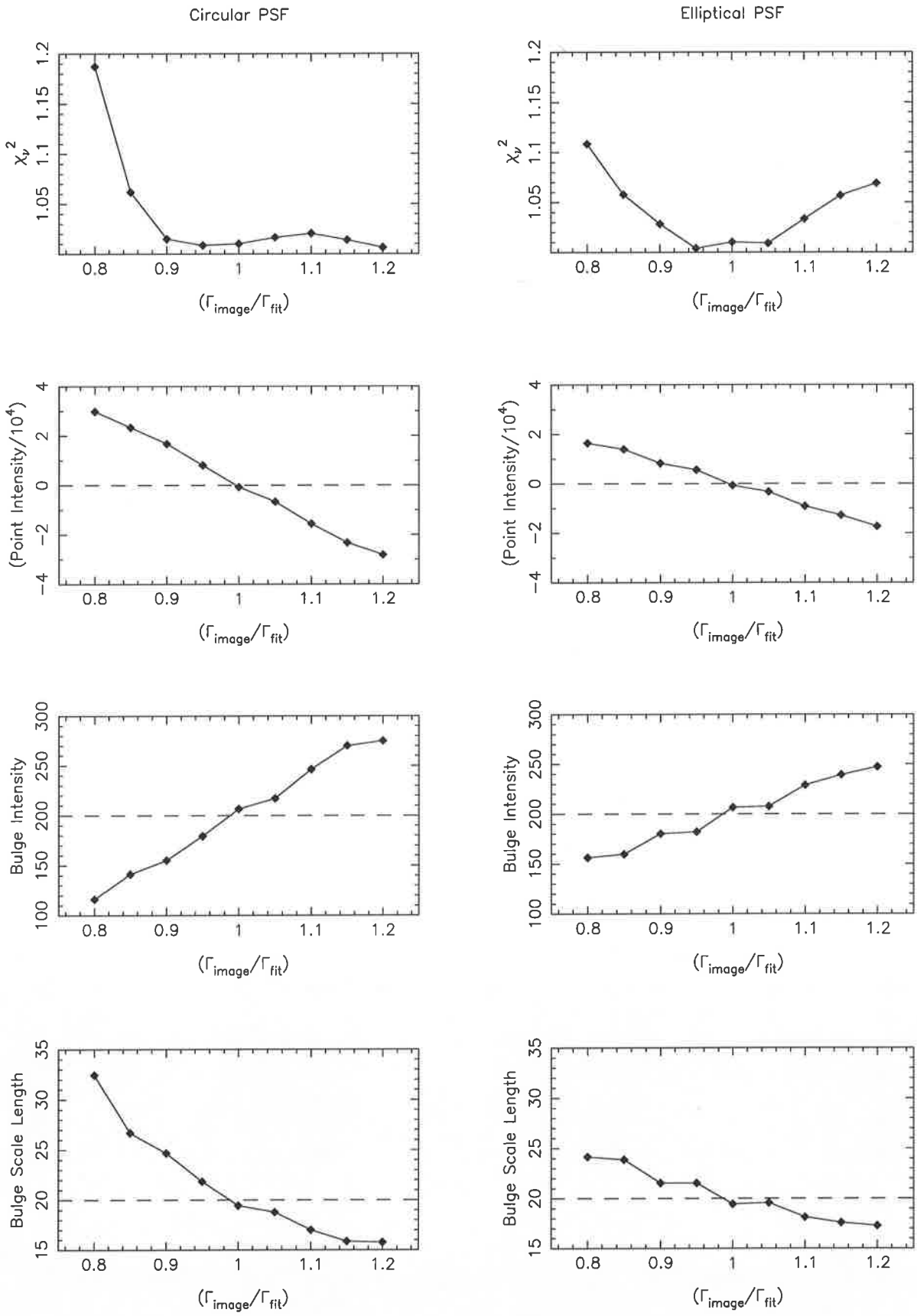

Fig. 3.— Effects of incorrect estimation of PSF on extracted parameters. The panels show changes in point intensity, bulge intensity and bulge scale length under a changing circular PSF (left panels) and changing

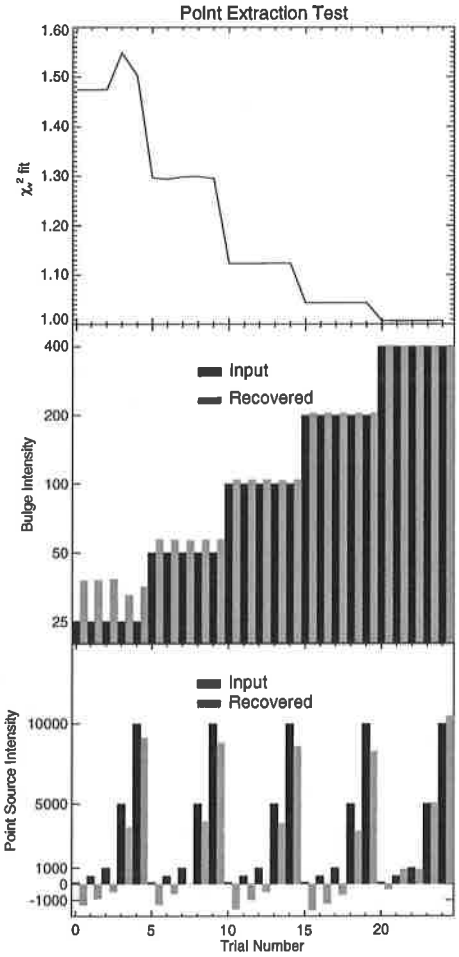

Fig. 4.— Results of point source extraction in 25 runs. The top panel shows the χ^2_ν value obtained in 25 runs. The bulge intensity increases after every 5 runs, resulting in a steep drop in χ^2, due to improved S/N ratio. The middle panel shows 25 input values for bulge intensity and the corresponding recovered value adjacent to each other. The lowest panel shows input point source intensities for each run and the corresponding recovered value. Note that the middle panel has the Y axis plotted on a logarithmic scale. See the text for further explanation.